Special issue: ICCESEN-2019

# Impact of Critical Plasma Spraying Parameter (CPSP) on Plasma-Sprayed $Al_2O_3$–3 $TiO_2$ Coatings

M. Djendel[a,b,*], O. Allaoui[b], M. Maazouz[c] and R. Boubaaya[a,b]

[a]Department of Science and Technics, Faculty of Technology, University of Bordj Bou Arreridj, Algeria

[b] Laboratoire Génie des Procédés, Université de Laghouat, BP 37G, Laghouat, Algérie

[c]Département de Génie Mécanique, Faculté de Technologies, Université de M'Sila, BP 166, M'Sila, Algérie

Atmospheric plasma spray (APS) coatings are successfully used in many industrial applications, where high wear and corrosion resistance with thermal insulation are required. Critical plasma spraying parameters (CPSP) is a key factor to control the quality of coatings. In this study, alumina–3 wt% titania coatings were prepared by APS torch at three different CPSP conditions (384.09, 469.44, and 563.33) on AISI 304 L stainless steel substrate. The microstructure, sliding wear rates, and porosity of the alumina–3 wt% titania composite coatings were investigated and correlated to CPSP conditions. The obtained results show that increasing the critical plasma spraying parameters increases the hardness and anti-wear behaviour of alumina–3 wt% titania coating.

DOI: 10.12693/APhysPolA.137.505

PACS/topics: Plasma spray, Coatings, Porosity, Wear behaviour, CPSP

## 1. Introduction

Plasma sprayed $Al_2O_3/TiO_2$ coatings have been widely used as wear resistance coatings in textile, machinery, and printing industries [1–2]. In process of plasma spraying, feedstock powder is melted and accelerated to high velocities (100 m/s), impinging upon the substrate, and rapidly solidifying (from 105 to 106 k/s) to create a "splat" [3, 7, 9]. The deposit develops by successive impingement and inter-bonding among the splats. The deposit microstructure is strongly dependent on processing conditions, spray parameters and feedstock materials. Many plasma spraying parameters influence the microstructure and physical properties of the coating [5, 10]. One can list, in particular, input power, plasma forming and secondary gas flow rate, standoff distance, transverse speed, carrier gas flow and powder feed rates, angle and location of powder injection-port and spraying angle directly or indirectly, influence the microstructure and physical properties of the coating [5, 10]. However, plasma torch input power and plasma forming gas flow rate are main parameters to control the nature of coatings. Some researchers have combine these two parameters, and introduced the critical plasma spraying parameter (CPSP) for coating optimization. This critical plasma spraying parameter (CPSP) with units [V A/Lpm] is defined as [4, 5]:

$$\text{CPSP} = \frac{\text{Voltage} \times \text{Current}}{\text{Primary gas flow rate}}. \tag{1}$$

Above formula contains the plasma output power in the numerator, and the primary gas (here Ar) flow rate in the denominator. Moreover, this variable is widely used to quantitatively identify the temperature of spray powders inside the plasma flame [15].

It is well known that when the plasma output power is increased, the particle temperature increases as well. It is due to increasing plasma jet temperature because it is very sensitive to CPSP. The decrease in the argon flow rate, which leads to an increase in the powder in-flight time, has a similar effect on the particle temperature as the increase in the plasma output power. Therefore, CPSP can alter the coating microstructure and properties, but is not the only way to adjust the coating microstructure and properties. In this study, we have studied the influence of CPSP on the microstructure, sliding wear rate, hardness and porosity (%) of the plasma sprayed of alumina–3 % titania coatings [8, 15].

## 2. Experimental procedure

### *2.1. Materials and coating deposition*

In this study AISI 304 stainless steel, substrate with 2 mm thickness, and 25 g/cm$^2$ density was selected as a substrate. The selected plate is a technical delivery conditions for general-purpose structural stainless steel, which is used to build ship, bridge, etc. Ceramic feedstock $Al_2O_3$–3 wt% $TiO_2$ was used as the main coating, while (Ni-20Cr)6Al powder was used as bond coating with an average of about 50 $\mu$m thick bond layer on the surface of the substrates to obtain better performance of the plasma sprayed $Al_2O_3$ — 3 $TiO_2$.

$Al_2O_3$–3 wt% $TiO_2$ coating was produced onto AISI 304 stainless steel substrate using Sulzer-Metco atmospheric plasma spray system 9MC Equipment, using argon and hydrogen as the plasma arc gases and argon as the powder carrier gas. Before coating, grid blasting of the steel samples was carried out using

*corresponding author; e-mail: djendelm@gmail.com

TABLE I

Chemical composition of $Al_2O_3$–3 wt% $TiO_2$ powder coating.

| Composition | $Al_2O_3$ | $TiO_2$ | $SiO_2$ | $Fe_2O_3$ | MgO | Others |
|---|---|---|---|---|---|---|
| wt% | 94.5 | 2.66 | 2.11 | 0.26 | 0.26 | 0.24 |

TABLE II

Plasma spraying conditions.

| Critical plasma spray parameters | 384.09, 469.44, and 563.33 |
|---|---|
| primary gas (Ar) flow rate | 80 L/min |
| secondary gas (He) flow rate | 50 L/min |
| powder carrier gas (Ar) flow rate | 30 L/min |
| powder flow rate | 10 g/min |
| spray distance | 100 mm |
| passes | 8 layer |
| spray angle | 90° |

a grid-blasting machine with 75–125 mm size sand at the air pressure of about 3.447 bar, at a distance of about ∼ 150 mm. The resulting average surface roughness was about 10 mm Ra. Subsequent to grid blasting, the samples were cleaned with forced air and acetone. Before coating process, the substrate was heated by plasma flame at a transverse speed of 500 mm/s and stand-off-distance at 100 mm for one pass, and the temperature of the substrate ranged between 100 °C and 200 °C. The chemical composition and powder size used as base materials are given in Table I. Further, the parameters of the plasma spraying conditions are summarized in Table II.

### *2.2. Characterization and analysis techniques*

For the microscopic observation and the microhardness measurements, the coated samples were cut for cross-section by using diamond wheel with a cutting speed of 20 mm/s and mounted metallographically before grinding and polishing. The samples were grounded with standard SiC grinding papers starting from 400 grid and finishing off with 1200 grid under constant load (5 N) and running duration (2 min). The samples were then lightly polished using 1 mm diamond paste.

Microhardness values of the specimens were taken from the cross-section of the polished samples at a‘ load of 2N using DM2D microhardness tester. The average values (ten points) of the measured microhardness are reported. The microstructure of the coatings was characterized by scanning electron microscopy (SEM). The phase composition of the coating was examined by X-ray diffraction (XRD).

### *2.3. Sliding wear*

The test method also called POD Test was performed by following the ASTM G99-95a Standard [12]. In this wear test, the coated sample was slid against 6 mm alumina ball. About 5 N load was applied to the contacted surface, and 3 mm radius was set from the centre. The sample was rotated at a speed 3.5 cm/s and slid for 500 m. During the test, the samples were tested at environment condition of 60% humidity and at 23 °C. Porosity in the coatings was determined by following ASTM standards C 20–92. In this research, the test for porosity is done additionally by weighing the specimens in the air and in the water using Mettler Toledo AG Balance.

## 3. Results and Discussion

### *3.1. CPSP effect on phase and microstructure*

Figure 1 shows the XRD patterns of the alumina–3 w% titania coatings performed at various CPSP conditions, i.e., 384.09, 469.44 and 563.33, which reveal a similar phase composition in all cases. Different phases of alumina exist in these plasma sprayed coatings: $\gamma$-$Al_2O_3$ is the predominant phase, and $\alpha$-$Al_2O_3$ is the minority phase, and diffraction lines of Rutile–$TiO_2$ could be identified.

The partial transformation of $\alpha$-$Al_2O_3$ to $\gamma$-$Al_2O_3$ in the deposited coatings is due to the plasma spray conditions and cooling process. The existence of $\gamma$-$Al_2O_3$ clearly indicates that the alumina in alumina–3% titania coatings is rapidly solidified process. In spite of the similarity among the various CPSP conditions of coatings, difference is obvious also when the intensities of XRD patterns are examined carefully. The crystallinity of each phase increases with CPSP, which results to enhance microstructure of the coatings. In addition, the presence of metastable phases of $Al_2TiO_5$ and $Ti_3O_5$ were identified. The formation of those phases increases while increasing CPSP. The $Al_2TiO_5$ and $Ti_3O_5$ phases have formed because of reaction between $TiO_2$ and $Al_2O_3$. However, the formation of $Al_2TiO_5$ and $Ti_3O_5$ phase depends on solubility of $TiO_2$ in $Al_2O_3$ structure and the process temperatures. It is known that the addition of $TiO_2$ to the $Al_2O_3$ coating is to reduce the melting

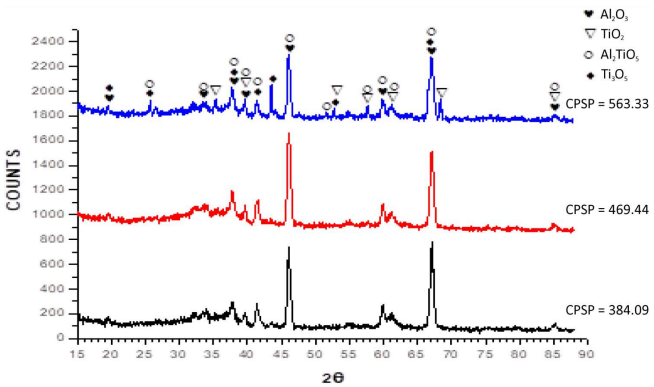


Fig. 1. XRD patterns of the alumina–3% titania coatings.

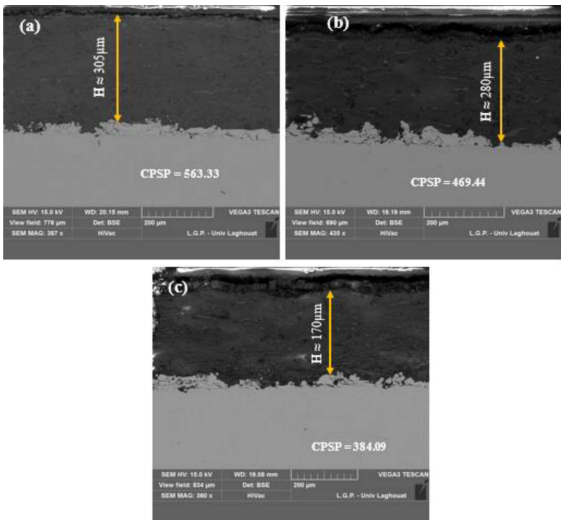


Fig. 2. SEM morphologies of the cross sections of as-sprayed coatings: (a) coating 1, (b) coating 2, and (c) coating 3.

temperature of the oxide, thereby producing less porous and better performance coatings than pure $Al_2O_3$ coatings [6, 14]. The decreased melting temperature is because $TiO_2$ has a lower melting temperature (1854 °C) than $Al_2O_3$ (2040 °C) and so its ability to form a liquid solution with $Al_2O_3$ [8].

SEM micrograph of $Al_2O_3$–3 wt% $TiO_2$ powder coating in Fig. 2 shows the morphology of coated samples of coating surface and cross-sectional view [13]. The coating samples had similar morphological features, as can be expected from their particle size distribution and the recommended spraying conditions at CPSP (384.09, 469.44 and 563.33). The coating features observe the molten particles condition and spread as out on top of the surface to develop coating layers. Some areas on the surface appear as semi-molten particles, and they agglomerate together with molten particle to form coating layers. The semi-molten particles exhibit pinholes, which are characteristic of porosity occurred on the coated sample. Based on the view of cross-section of top coating morphology, we identified that different coating thickness were produced. As shown in Fig. 2, the maximum thickness of the sprayed coatings varies from about 305 $\mu$m under CPSP = 563.33, to about 280 $\mu$m under CPSP = 469.44, and about 170 $\mu$m under CPSP = 384.09.

In addition, the coating 1 deposited at a low primary gas flow rate of 35 L/min seems to be incompact because of larger number of pores with a large volume (Fig. 2a). As the primary gas flow rate increases to 40 L/min, then the resultant of coating 2 contains fewer pores (Fig. 2b), which corresponds to its improved compactness. However, the coating 3 deposited at the high primary gas flow rate of 45 L/min contains a large amount of pores and seems to be more porous than the coating 2 (Fig. 2c).

### *3.2. CPSP effect on porosity level (%)*

Figure 3 shows the porosity level (%) of the plasma sprayed of alumina–3 wt% titania composite coatings as a function of CPSP conditions. In alumina–3 wt% titania, the porosity level decreases with increasing CPSP conditions. The coatings are formed by the piling of melted droplets. It is expected that before impact a higher particle velocity may give better spreading. Complete melting of the particles and higher velocity will yield lesser porosity in the coating. Hence increasing CPSP gives low porosity coatings. The occurred porosity also may be due to the lamellae structure, which exhibit molten and semi-molten particles, and will create pinholes inside the coating. The porosity may occur due to absorbed gases during spraying process.

### *3.3. CPSP effect on hardness and wear resistance*

Figure 4 show the microhardness of the plasma sprayed of alumina–3 wt% titania coatings as a function of CPSP conditions. The overall hardness increases in the order of the A1, A2, and A3 coatings as the CPSP increases.

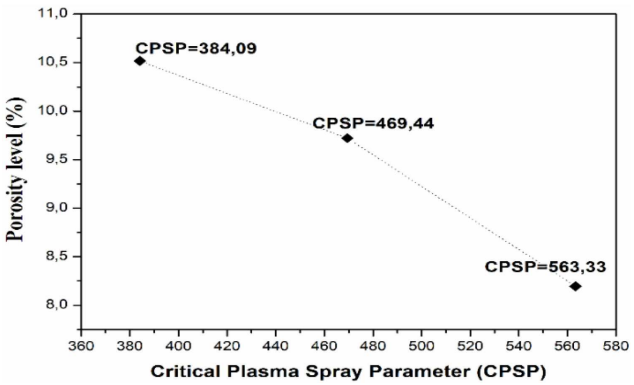


Fig. 3. Effect of CPSP on the porosity level (%) of the plasma sprayed alumina–3 wt% titania coatings.

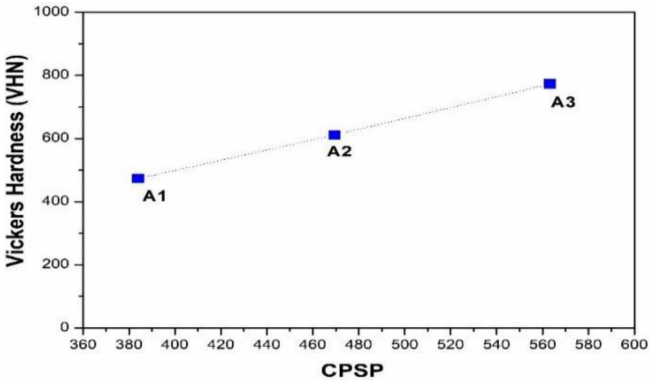


Fig. 4. Effect of CPSP on the micro-hardness of the plasma sprayed alumina–3 wt% titania composite coatings.

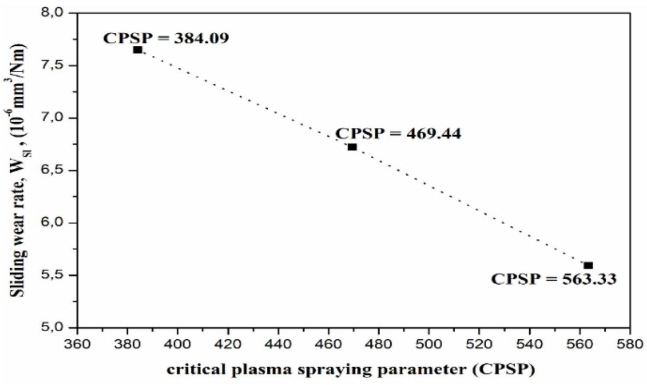


Fig. 5. Effect of CPSP on the sliding wear rate of the plasma sprayed alumina–3 wt% titania composite coatings.

The microhardness of the fully and partially melted regions ranges 470–600 VHN, and 790 VHN, respectively. In fact, these partially melted regions could play an important role in determining the overall hardness of the coatings because they are softer than the fully melted regions.

Figure 5 shows the sliding wear behavior of plasma sprayed of alumina–3 wt% titania coating at different CPSP conditions. The results indicate that the sliding wear rate decreases with increasing CPSP conditions.

## 4. Conclusion

Atmospheric plasma sprayed alumina–3 wt% titania composites coatings were prepared for different CPSP conditions (384.09, 469.44, 563.33) and their microstructure, hardness, and wear resistance were investigated. In this study, the following conclusions can be drawn.

The phases exist from $\alpha$-$Al_2O_3$ to $\gamma$-$Al_2O_3$ and SEM analysis for the ceramic coating shows that the $Al_2O_3$–3 wt% $TiO_2$ particles are enough melted, high dense, and they form a strong coating onto the substrates.

At CPSP 563.33, the alumina–3 wt% titania composite coating gives best sliding wear resistance, highest microhardness values, and lowest porosity.

In the POD test, the results show that if the coating hardness increased, wear behavior of coating samples decreased.

## References

[1] G. Güraksin, E. Biçer, A. Evcin, *Int. J. Comput. Exp. Sci. Eng. (IJCESEN)* **3 (2)**, 15 (2017).

[2] A. Günen, *Acta Phys. Pol. A* **130**, 217 (2016).

[3] H. Ageorges, P. Ctibor, *Surf. Coat. Technol.* **202 (18)**, 4362 (2008).

[4] M. Ozsoy, İ Tikiz, H. Pehlivan, *Int. J. Comput. Exp. Sci. Eng. (IJCESEN)* **4 (3)**, 43 (2018).

[5] XuMing-San, JeanMing-Der, *Emerg. Mater. Res.* **7(2)**, 73 (2018).

[6] L. Shaw, D. Goberman, M. Gell, S. Jiang, Y. Wang, T.D. Xiao, P. Strutt, *Surf. Coat. Technol.* **130**, 1 (2000).

[7] M. Djendel, O. Allaoui, A. Bouzid, *Int. J. Comput. Exp. Sci. Eng. (IJCESEN)* **2(2)**, 1 (2016).

[8] M.S.A. Rahim, S.N. Hayati, H.L. Bakir, *Int. J. Precision Technol.* **1(2)**, 163 (2009).

[9] A.-F. Kanta, M.-P. Planche, G. Montavon, C. Coddet, *Surf. Coatings Technol.* **204**, 1542 (2010).

[10] P. Fauchais, A. Vardelle, B. Dussoubs, in: *Thermal Spray 2001, New Surfaces for a New Millennium*, Eds. C.C. Berndt, K.A. Khor, E.F. Lugscheider, ASM International, Materials Park (OH) 2001, p. 1.

[11] İ.H. Karahan, *Acta Phys. Pol. A* **128**, B-432 (2015).

[12] R.R. Bajmalu, T. Mohammad, *Emerg. Mater. Res.* **6(1)**, 160 (2017).

[13] M. Djendel, O. Allaoui, R. Boubaaya, *Acta Phys. Pol. A* **132**, 538 (2017).

[14] A. Haghighatzadeh, B. Mazinani, A. Salari, *Acta Phys. Pol. A* **132** , 538 (2017).

[15] E.H. Jordan, M. Gell, Y.H. Sohn, D. Goberman, L. Shaw, S. Jiang, M.Wang, T.D. Xiao, Y. Wang, P. Strutt, *Mater. Sci. Eng.* **A301**, 80 (2001).